Article

Design of a Calcium-Binding Protein with Desired Structure in a Cell Adhesion Molecule

Wei Yang, Anna L. Wilkins, Yiming Ye, Zhi-ren Liu, Shun-yi Li, Jeffrey L. Urbauer, Homme W. Hellinga, Alice Kearney, P. Anton van der Merwe, and Jenny J. Yang

J. Am. Chem. Soc., **2005**, 127 (7), 2085-2093• DOI: 10.1021/ja0431307 • Publication Date (Web): 29 January 2005

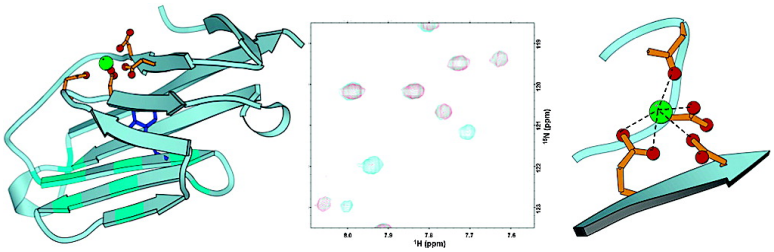

More About This Article

Additional resources and features associated with this article are available within the HTML version:

- Supporting Information
- Links to the 4 articles that cite this article, as of the time of this article download
- Access to high resolution figures
- Links to articles and content related to this article
- Copyright permission to reproduce figures and/or text from this article

View the Full Text HTML

J|A|C|S
ARTICLES
Published on Web 01/29/2005

Design of a Calcium-Binding Protein with Desired Structure in a Cell Adhesion Molecule

Wei Yang,[†] Anna L. Wilkins,[†] Yiming Ye,[†] Zhi-ren Liu,[‡] Shun-yi Li,[†]
Jeffrey L. Urbauer,[§] Homme W. Hellinga,[¶] Alice Kearney,[#]
P. Anton van der Merwe,[#] and Jenny J. Yang*,[†]

Contribution from the Departments of Chemistry and Biology, Center for Drug Design and Biotechnology, Georgia State University, Atlanta, Georgia 30303, Department of Chemistry, University of Georgia, Athens, Georgia 30602-2556, Department of Biochemistry, Medical Center, Duke University, Durham, North Carolina 27710, and Sir William Dunn School of Pathology, University of Oxford, South Parks Road, Oxford, OX1, 3RE, U.K.

Received November 15, 2004; E-mail: cherry@langate.gsu.edu; chejjy@panther.gsu.edu.

Abstract: Ca^{2+}, "a signal of life and death", controls numerous cellular processes through interactions with proteins. An effective approach to understanding the role of Ca^{2+} is the design of a Ca^{2+}-binding protein with predicted structural and functional properties. To design de novo Ca^{2+}-binding sites in proteins is challenging due to the high coordination numbers and the incorporation of charged ligand residues, in addition to Ca^{2+}-induced conformational change. Here, we demonstrate the successful design of a Ca^{2+}-binding site in the non-Ca^{2+}-binding cell adhesion protein CD2. This designed protein, Ca·CD2, exhibits selectivity for Ca^{2+} versus other di- and monovalent cations. In addition, La^{3+} (K_d 5.0 μM) and Tb^{3+} (K_d 6.6 μM) bind to the designed protein somewhat more tightly than does Ca^{2+} (K_d 1.4 mM). More interestingly, Ca·CD2 retains the native ability to associate with the natural target molecule. The solution structure reveals that Ca·CD2 binds Ca^{2+} at the intended site with the designed arrangement, which validates our general strategy for designing de novo Ca^{2+}-binding proteins. The structural information also provides a close view of structural determinants that are necessary for a functional protein to accommodate the metal-binding site. This first success in designing Ca^{2+}-binding proteins with desired structural and functional properties opens a new avenue in unveiling key determinants to Ca^{2+} binding, the mechanism of Ca^{2+} signaling, and Ca^{2+}-dependent cell adhesion, while avoiding the complexities of the global conformational changes and cooperativity in natural Ca^{2+}-binding proteins. It also represents a major achievement toward designing functional proteins controlled by Ca^{2+} binding.

Introduction

Ca^{2+} regulates many biological processes through its interactions with Ca^{2+}-receptor/binding proteins.[1] Multiple Ca^{2+}-binding proteins with different Ca^{2+}-binding affinities have been identified in various cellular environments in all eukaryotic cells.[2] Extracellularly, Ca^{2+} interacts with numerous Ca^{2+}-dependent receptors and cell adhesion molecules, with affinities between 0.1 and 10 mM, corresponding to the Ca^{2+} concentration in circulating fluids, which are essential for signal transduction, Ca^{2+}-dependent cell adhesion, and their proteolytic stability.[3,4] Intracellularly, Ca^{2+}-binding proteins have Ca^{2+}-binding affinities in the submicromolar range. For example, four Ca^{2+} ions cooperatively bind to calmodulin to induce a large conformational change that, in turn, results in the regulation of a number of proteins that bind the $Ca^{2+}-$CaM proteins.[5,6] A major barrier to understanding the molecular mechanism of Ca^{2+}-dependent biological function is the lack of established rules relating Ca^{2+} binding with specific structural aspects of proteins. This is exacerbated by the complexities encountered in cooperative, multisite systems and the use of Ca^{2+}-binding energy for conformational changes in proteins. Understanding the role of Ca^{2+} in the regulation of adhesion function is particularly difficult because of the Ca^{2+}-induced oligomerization.[7]

An effective approach to understanding the role of Ca^{2+} is the de novo design of a Ca^{2+}-binding protein with predicted structural and functional properties. Designing a single Ca^{2+}-binding site into a functional protein without a global conformational change is particularly advantageous for understanding the key factors contributing to Ca^{2+} binding.[8] Therefore, the Ca^{2+}-binding properties can be directly correlated with local structural features, such as coordination ligands, number of

[†] Department of Chemistry, Georgia State University.
[‡] Department of Biology, Georgia State University.
[§] University of Georgia.
[¶] Duke University.
[#] University of Oxford.

(1) Berridge, M. J.; Bootman, M. D.; Lipp, P. *Nature* **1998**, *395*, 645−648.
(2) Glusker, J. P. *Adv. Protein Chem.* **1991**, *42*, 1−76.
(3) Brown, E. M.; MacLeod, R. J. *Physiol. Rev.* **2001**, *81*, 239−297.
(4) Shapiro, L.; Colman, D. R. *Curr. Opin. Neurobiol.* **1998**, *8*, 593−599.
(5) Kawasaki, H.; Kretsinger, R. H. *Protein Profile* **1995**, *2*, 297−490.
(6) Nelson, M. R.; Chazin, W. J. *Biometals* **1998**, *11*, 297−318.
(7) Nagar, B.; Overduin, M.; Ikura, M.; Rini, J. M. *Nature* **1996**, *380*, 360−365.
(8) Yang, W.; Jones, L. M.; Isley, L.; Ye, Y.; Lee, H. W.; Wilkins, A.; Liu, Z. R.; Hellinga, H. W.; Malchow, R.; Ghazi, M.; Yang, J. J. *J. Am. Chem. Soc.* **2003**, *125*, 6165−6171.

10.1021/ja0431307 CCC: $30.25

charged ligand residues, and geometry of the metal-binding sites. Moreover, these studies are a prelude for more sophisticated ones to design Ca^{2+}-dependent proteins by introduction of Ca^{2+}-binding sites to ultimately control function.

The rational design of binding sites with a strong selectivity for Ca^{2+} is, however, extremely challenging because of the complexity and irregularity of such sites and the likelihood of altered protein conformation resulting from the introduction of charged residues. Ca^{2+}-binding ligands in proteins usually contain oxygen atoms from different sources, such as the side chain carboxylates and hydroxyls, the main chain carbonyl, and water molecules. Ca^{2+} binding requires a higher coordination number, normally 6−7, compared to 4 for other metal ions with less regularity in bond lengths and angles.[9] Furthermore, several charged residues required in the primary coordination of the binding shell may alter the structure and function of the protein. Therefore, it is essential to establish a general methodology for designing Ca^{2+}-binding proteins and to provide a clearer view of the structural determinants that are necessary for a functional protein to accommodate the metal-binding site.

We have developed a novel approach for the de novo design of a single Ca^{2+}-binding site within non-Ca^{2+}-binding proteins[10] without splicing in an entire, known metal-binding domain.[11,12] By taking into account the local coordination properties of Ca^{2+}-binding sites in natural Ca^{2+}-binding proteins and chelators, we have previously shown that the resulting proteins selectively bind Ca^{2+} and the Ca^{2+} analogues, La^{3+} and Tb^{3+}.[8,13] Unfortunately, this first group of designed Ca^{2+}-binding proteins was unstable and did not retain the native fold and original protein function, so it was impossible to further characterize these proteins by high-resolution structural analysis methods. In the current study, we report a general strategy for rationally designing stable Ca^{2+}- and Ln^{3+}-binding proteins that retain the biological function of the host protein. To create a model system to study Ca^{2+}-dependent cell adhesion by protein design, we have chosen domain 1 of CD2 as a scaffold protein. CD2 enhances T cell and NK cell activation by interacting with CD48 or CD58 on the antigen-presenting cells and is one of the most extensively studied non-Ca^{2+}-binding cell adhesion proteins.[14−19] We have converted CD2 into a specific receptor for Ca^{2+} (Ca·CD2) (Figure 1). Our NMR structural determination reveals that Ca^{2+} binds specifically to the designed Ca^{2+}-binding residues in Ca·CD2 (Figure 1). The introduction of the Ca^{2+}-binding site into CD2 does not alter its overall native structure or its ability to bind its natural ligand (CD48) or the conformation-dependent antibodies (OX34 and OX55). Our first success in designing a Ca^{2+}-binding protein with desired structural and functional properties opens a new avenue in unveiling key determinants to Ca^{2+}-binding affinity, the mechanism of Ca^{2+} signaling, and Ca^{2+}-dependent cell adhesion, while avoiding the complexities of the global conformational changes, cooperativity, and the multibinding process found in natural Ca^{2+}-binding proteins. It demonstrates the potential to design novel Ca^{2+}-dependent proteins with specifically tailored functions.

Experimental Methods

Design Process. The survey of key features of Ca^{2+}-binding sites was carried out using natural-evolved Ca^{2+}-binding proteins and small chelators.[10,20] The protein design is carried out on an SGI O2 computer using the MetalFinder program modified on Dezymer.[10,20] The CD2 protein (1hng)[18] was chosen as the host for the Ca^{2+}-binding site. One bidentate aspartate and three unidentate ligands from glutamate, aspartate, asparagine, glutamine, threonine, serine, and/or main chain carbonyl are used for the calculation. The parameters derived from ideal pentagonal bipyramidal geometry are used to create Ca^{2+}-binding sites. Two remaining positions are left empty for water. The constructed sites are then minimized based on the ideal geometry.

The potential Ca^{2+}-binding sites were evaluated and analyzed for their coordination properties and protein environment according to key features of geometric and chemical properties of the metal-binding sites surveyed. Any sites requiring the mutation of buried hydrophobic residues and key positions for folding, such as W32, I18, and V78,[21] were eliminated. The constructed sites were ranked by our program PROTEUS according to the number of mutations required, the number of charged residues, and the solvent accessibility of the ligand residues.

Protein Engineering and Purification. Ca·CD2 and its variants were cloned by standard PCR reactions from rat CD2 DNA. Homonuclear and ^{15}N-labeled proteins were expressed in LB and SV minimal media, respectively. All proteins were purified using a modified protocol for CD2 variants.[8]

Terbium-Sensitized Fluorescence Resonance Energy Transfer. Aromatic residue Tb^{3+} fluorescence energy transfer experiments were performed using a PTI fluorimeter equipped with a Hamilton Microlab 500 series for titration with our established protocol.[8]

NMR Spectra. All NMR spectra were recorded using a Varian 500, 600, or 800 MHz spectrometer with a spectral width of about 13 ppm in the ^1H dimension and 36 ppm in the ^{15}N dimension. The samples were in 20 mM PIPES/130 mM KCl, pH 6.8, with either EGTA (1−3 mM) or Ca^{2+} (10 mM), unless otherwise specified. The protein concentrations were 1 mM for homonuclear 2D and ^{15}N-evolved 3D spectra and 0.2−0.3 mM for 1D and HSQC spectra. In 1D spectra, EGTA, K^+, Mg^{2+}, and Ca^{2+} were sequentially added into the same protein sample to achieve the final concentrations of 0.050, 130, 10, and 5 mM, respectively.

The Ca^{2+}-binding affinity of Ca·CD2 was measured by monitoring the ^1H chemical shift changes versus the Ca^{2+} concentrations in the HSQC spectra in 10 mM Tris/10 mM KCl, pH 7.4, with 50 μM EGTA at the starting point. As the Ca^{2+} concentration was much greater than the protein concentration, the total Ca^{2+} concentration was assumed to be the free Ca^{2+} concentration during the titration process. Examination of the resulting spectra indicates a two-process change induced by Ca^{2+}. For example, L63 initially moved downfield before moving upfield; the movement of I18 followed a curved path (Figure 2a). Therefore, the data were fitted using an equation derived from a two-process binding:

$$\Delta S = \frac{\Delta S_1 \times [\mathrm{Ca}]}{K_{d1} + [\mathrm{Ca}]} + \frac{\Delta S_2 \times [\mathrm{Ca}]}{K_{d2} + [\mathrm{Ca}]}$$

(9) Pidcock, E.; Moore, G. R. *J. Biol. Inorg. Chem.* **2001**, *6*, 479−489.
(10) Yang, W.; Lee, H. W.; Hellinga, H.; Yang, J. J. *Proteins* **2002**, *47*, 344−356.
(11) Kuroki, R.; Taniyama, Y.; Seko, C.; Nakamura, H.; Kikuchi, M.; Ikehara, M. *Proc. Natl. Acad. Sci. U.S.A.* **1989**, *86*, 6903−6907.
(12) Toma, S.; Campagnoli, S.; Margarit, I.; Gianna, R.; Grandi, G.; Bolognesi, M.; De Filippis, V.; Fontana, A. *Biochemistry* **1991**, *30*, 97−106.
(13) Wilkins, A. L.; Ye, Y.; Yang, W.; Lee, H. W.; Liu, Z. R.; Yang, J. J. *Protein Eng.* **2002**, *15*, 571−574.
(14) Davis, S. J.; Davies, E. A.; Tucknott, M. G.; Jones, E. Y.; van der Merwe, P. A. *Proc. Natl. Acad. Sci. U.S.A.* **1998**, *95*, 5490−5494.
(15) Leahy, D. J. *Annu. Rev. Cell Dev. Biol.* **1997**, *13*, 363−393.
(16) Wang, J. H.; Smolyar, A.; Tan, K.; Liu, J. H.; Kim, M.; Sun, Z. Y.; Wagner, G.; Reinherz, E. L. *Cell* **1999**, *97*, 791−803.
(17) Driscoll, P. C.; Cyster, J. G.; Campbell, I. D.; Williams, A. F. *Nature* **1991**, *353*, 762−765.
(18) Jones, E. Y.; Davis, S. J.; Williams, A. F.; Harlos, K.; Stuart, D. I. *Nature* **1992**, *360*, 232−239.
(19) Wagner, G.; Wyss, D. F. *Curr. Opin. Struct. Biol.* **1994**, *4*, 841−851.
(20) Hellinga, H. W.; Richards, F. M. *J. Mol. Biol.* **1991**, *222*, 763−785.
(21) Parker, M. J.; Dempsey, C. E.; Hosszu, L. L.; Waltho, J. P.; Clarke, A. R. *Nat. Struct. Biol.* **1998**, *5*, 194−198.

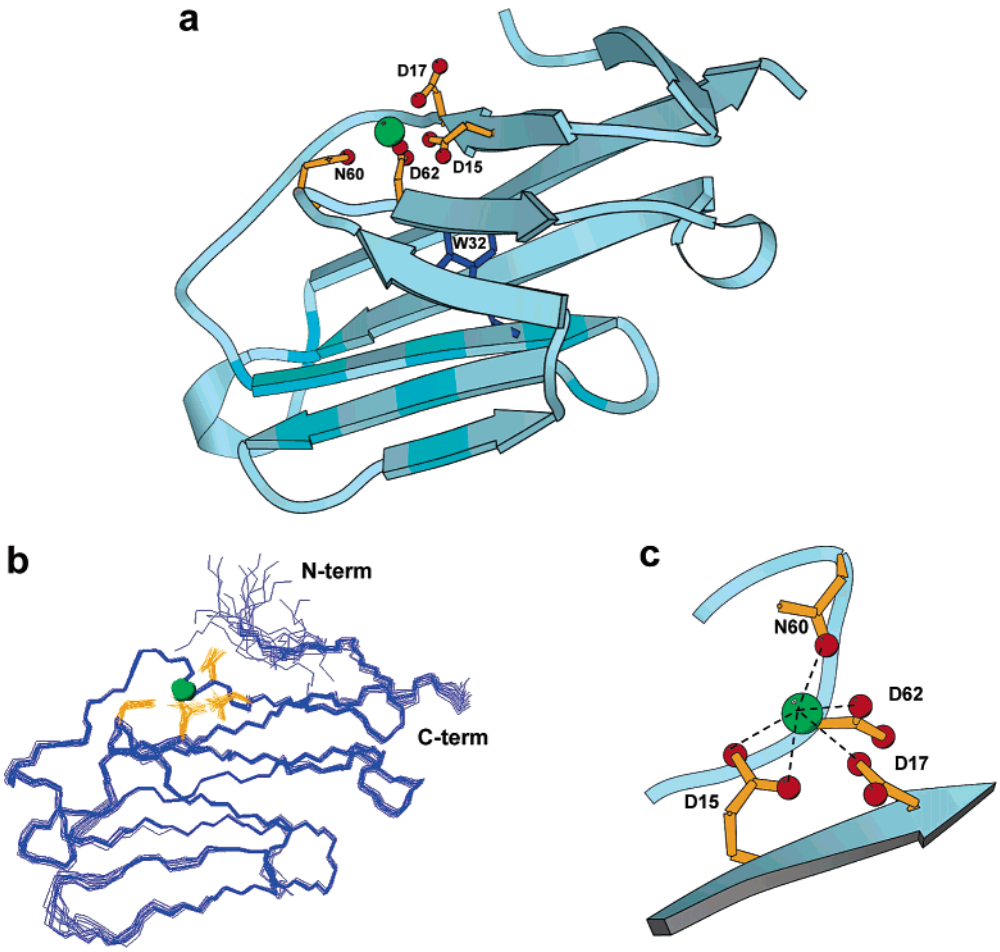

Figure 1. Solution structure of Ca·CD2 has been deposited in the protein data bank with an accession code of 1T6W. (a) Average solution structure of Ca·CD2. The designed Ca^{2+}-binding site includes ligand residues with yellow side chains (D15, D17, N60, and D62). Ca^{2+} is shown as a green sphere. Trp-32 (blue) is located proximally to this binding pocket. Residues that are involved in the recognition of CD48 are highlighted in cyan. (b) Backbone superposition of the 20 simulated annealing structures of Ca·CD2 with the lowest energy, generated by superimposing the backbone of residues 6−98 using MolMol.[35] (c) One example of the Ca^{2+}-binding pocket in the solution structure of Ca·CD2, consistent with the designed pentagonal bipyramidal geometry. Figures 1a and 1c are prepared using MOLSCRIPT.[36]

where the total signal change (ΔS) is the sum of the change from the first process (ΔS_1) and the second process (ΔS_2), and K_{d1} and K_{d2} are the dissociation constants for these two processes, respectively. By monitoring the changes of D17, I18, D62, and L63, we determined the Ca^{2+}-binding affinity of the designed site (1.4 ± 0.4 mM). The K_d of the second process (15 ± 5 mM) was similar to the values (10−20 mM) obtained from the non-Ca^{2+}-binding residues (F21, Q22, K43, and K66), suggesting that the second process is nonspecific.

For the Mn^{2+}-relaxation investigation, the HSQC spectra were collected with and without 50 μM Mn^{2+} in the presence of 0.2 mM Ca·CD2, 50 mM PIPES, 130 mM KCl, 1 mM $CaCl_2$, pH 6.8 at 4 °C. To investigate the distance effect of Mn^{2+}, the logarithmic plot of the Δi^{-1} values around the Ca^{2+}-binding pocket versus the distance of the corresponding amide proton to the metal was generated, where the distance was calculated using the average solution structure and the Δi^{-1} is the intensity ratio of the peaks with and without 20 μM Mn^{2+} in 50 mM PIPES, 130 mM KCl, pH 6.8.[22,23]

Structure Calculation. The assignment of NMR spectra was achieved by standard methods and procedures. During the initial structural calculation, only the distance constraints derived NOEs were input into the CNS algorithm. The H-bond constraints were added into the calculation in a later running based on the prestructures and the amide proton chemical shift difference between Ca·CD2 and CD2. Residues that have chemical shift differences smaller than 0.05 ppm were assumed to maintain H-bond as in the CD2 (analyzed using the crystal structure 1HNG). Five constraints that restrict the Ca−O distance between the Ca^{2+} and the ligand oxygen were included in the final calculation based on the statistic survey and supported by the Mn^{2+}-relaxation results.

Biacore Measurement. Surface plasmon resonance studies were performed at 25 °C with a flow rate of 10 mL/min using a Biacore 2000 (BIAcore AB, Stevenage, Herts, U.K.) in HBS buffer containing either EGTA or $CaCl_2$. The anti-GST (Glutathione S-Transferase) antibody was coupled to a CM5 sensor chip using the amine coupling kit as directed, with the following modifications. After an activation step of 300 s, anti-GST antibody (30 μg/mL in sodium acetate, pH 5.0) was injected for 300 s. Immobilization levels were approximately 17 000 RU (response units). The anti-GST antibody was regenerated with 10 mM glycine/HCl, pH 2.0 (Biacore). The GST-fusion proteins were all diluted $^1/_{10}$ in HBS buffer and injected for 180 s over the immobilized anti-GST antibody. Affinity measurements were performed as previously described using soluble rat CD48.[14] Monoclonal anti-rat antibodies were diluted to 100 μg/mL and injected for 300 s.

Results and Discussion

Strategy of Protein Design and Evaluation. A general strategy has been developed for designing de novo Ca^{2+}-binding protein with desired structural and functional properties. This strategy involves three major steps: surveying, creating, and

(22) Dahiyat, B. I.; Mayo, S. L. *Science* **1997**, *278*, 82−87.
(23) Ubach, J.; Zhang, X.; Shao, X.; Sudhof, T. C.; Rizo, J. *EMBO J.* **1998**, *17*, 3921−3930.

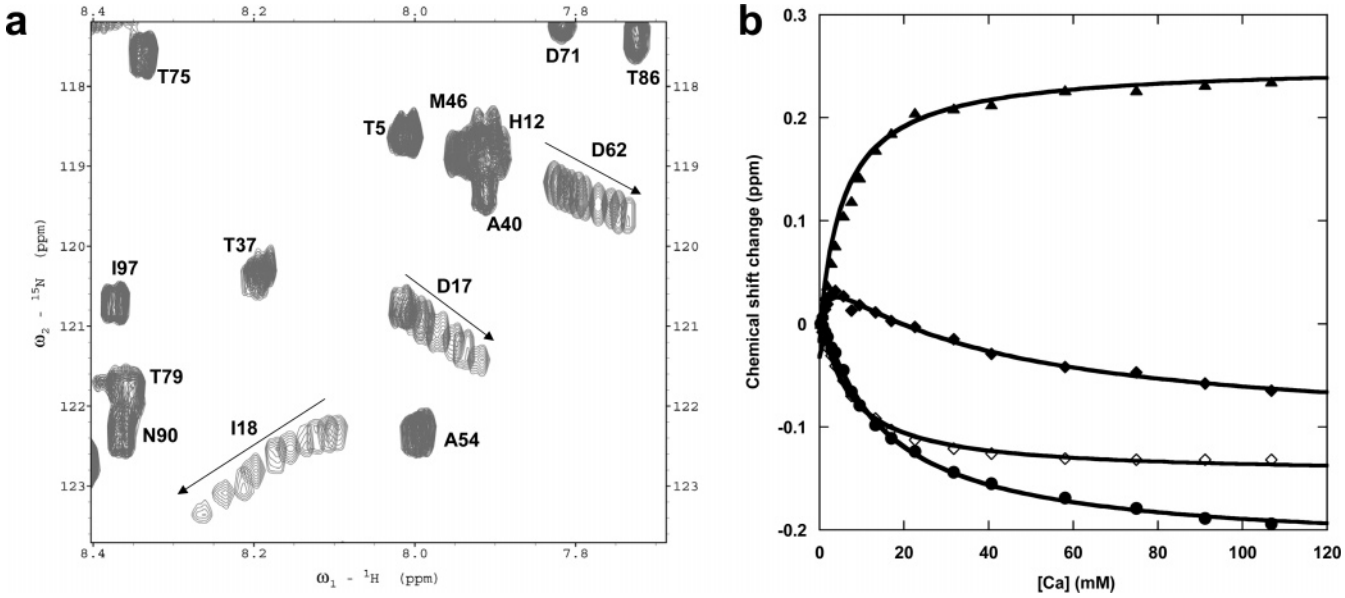

Figure 2. Ca^{2+}-binding affinity of Ca·CD2. (a) Ca^{2+} titration of Ca·CD2 (0.3 mM) in 10 mM Tris, 10 mM KCl at pH 7.4. Only the cross-peaks of D17, I18, and D62 shift, as the arrows indicate. (b) Ca^{2+}-binding affinity (1.4 ± 0.4 mM) was obtained by monitoring the proton chemical shift changes of D17 (●), I18 (▲), D62 (◊), and I63 (♦) fitting (—) with a model of two-phase Ca^{2+} binding. An additional process was due to the nonspecific binding also observed in F21, Q22, K43, K66, and other non-Ca^{2+}-binding residues (data not shown).

evaluating. First, the key features of geometric and chemical properties of the binding sites are revealed by surveying the binding sites in the structural banks for small chelators and proteins. Specifically, structural parameters of the coordination geometry are derived based on the analysis of the bond angles and lengths encompassing the metal-binding sites. Chemical properties at the local coordination, such as the types of ligand atoms (e.g., oxygen atoms for Ca^{2+}), the number of charged residues, and their arrangement (electrostatic distributions), are examined. The Ca^{2+}-binding preferences of each type of ligand residue (main chain carbonyl, solvent water, or side chain carboxyl groups) are ranked according to their frequency in the databanks surveyed. In addition, the solvent accessibility, the second shell interactions, such as hydrogen bonding and salt bridges of the ligand residues to the nearby residues, and the structural locations of ligand residues are further examined. Second, using a computer algorithm, potential Ca^{2+}-binding sites were created within the backbone structure of the non-Ca^{2+}-binding protein. The established geometric description for a Ca^{2+}-binding site and a library of side chain rotamers of ligand residues (or atoms from the main chain) with strong Ca^{2+}-binding preferences were applied.[8,13,14] Third, these potential Ca^{2+}-binding sites are then evaluated according to key features of the geometric and chemical properties of the metal-binding sites from the survey. Constructed sites involving mutations of residues at conserved positions and residues essential for folding and biological functions of the scaffold protein are automatically eliminated from further consideration.[8,13,14]

To create a model system to study Ca^{2+}-dependent cell adhesion by protein design, we have chosen domain 1 of CD2 as a scaffold protein. CD2 is one of the most extensively studied non-Ca^{2+}-binding cell adhesion proteins.[14−18] Through specific interactions with its ligand (e.g., CD48 for rat, CD58 for human), CD2 enhances T cell and NK cell activation by interacting with CD48 or CD58 on the antigen-presenting cells.[14,16,18,19] The binding site for CD48 is on the AGFCC′C″ surface of domain 1 of CD2, and charge−charge interactions contribute to the specificity.[14] To convert CD2 into a Ca^{2+} receptor, we have computationally designed single Ca^{2+}- binding sites within the backbone of domain 1 of CD2 (1hng) using the common pentagonal bipyramidal geometry based on our previous structural analysis and survey (Experimental Methods). The generated potential Ca^{2+}-binding sites (∼10 000) were then minimized based on the target geometry.[8,13,14] The designed Ca^{2+}-binding site in CD2 (Ca·CD2) was finally selected after careful evaluation. As shown in Figure 1a, this designed Ca^{2+}-binding site is formed by two discontinuous sections of the polypeptide and includes the oxygens from the side chains of Asp and Asn (D15 and D17 at β-strand B and N60 and D62 at the DE loop). There are three negatively charged Asp at the primary coordination shell. All other charged residues are more than 10 Å away from the binding pocket with the exception of K64, which is approximately 6 Å away from D15 and D62. Asp and Asn were selected as Ca^{2+} ligand residues because Ca^{2+} prefers Asp over Glu for binding, especially for the discontinuous Ca^{2+}-binding motifs in nonhelical proteins.[9] Asn is the most common noncharged Ca^{2+}-binding ligand residue. In addition, Asp can serve as either a unidentate or bidentate Ca^{2+} ligand. All of the ligand residues are at the surface of the protein with excellent solvent accessibility to accommodate electrostatic interactions between Ca^{2+} and its charged ligand residues and to facilitate water as ligand atoms. In addition, this designed Ca^{2+}-binding site utilizes existing side chain oxygen atoms from N60 and D62 as Ca^{2+} ligands so that mutation and potential structural alteration are avoided. Finally, to achieve desired functional properties, such as maintaining original cell adhesion properties of CD2, we have tailored the designed Ca^{2+}-binding site to this location on the opposite side of the functional cell adhesion surface of CD2 to prevent direct interference with the molecular recognition surface for CD48.

Metal-Binding Affinity and Selectivity. The affinities of Ca·CD2 for mono- and divalent cations were examined using several techniques. In the two-dimensional $^1H-^{15}N$ HSQC spectra, the majority of the resonances of Ca·CD2 are not

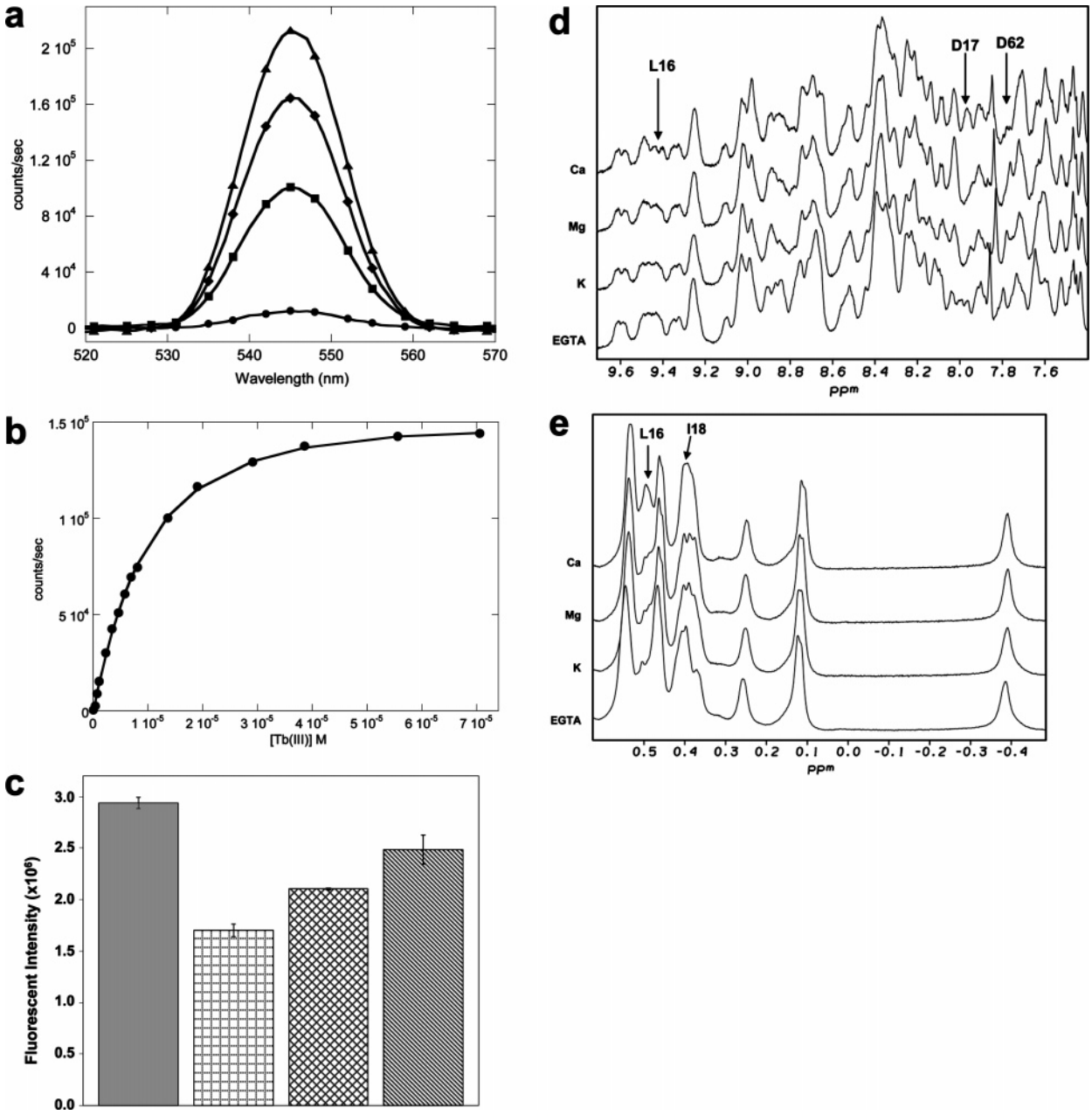

Figure 3. Metal-binding properties and selectivity of Ca·CD2. (a) Fluorescence emission spectra of 30 μM Tb^{3+} in the presence of 0 (●), 2 (■), 4 (♦), and 5 (▲) μM Ca·CD2 (excited at 282 nm) in 20 mM PIPES/10 mM KCl, pH 6.8. (b) Global fitting of Tb^{3+} fluorescence enhancement (500−600 nm) as a function of Tb^{3+} concentration using Specfit/32 (Spectrum Software Associates). (c) Competition study of 6 μM Ca·CD2 with 30 μM Tb^{3+} only (gray), in the presence of 100 μM La^{3+} (square), 10 mM Ca^{2+} (crosshatch), and 10 mM Mg^{2+} (diagonal) in 20 mM PIPES/10 mM KCl, pH 6.8. Fluorescent intensities are accumulated area from 527 to 568 nm. (d) Amide and (e) side chain regions of 1D ^{1}H NMR spectra of Ca·CD2 (200 μM) with sequential addition of 0.050 mM EGTA, 130 mM KCl, 10 mM $MgCl_2$, and 5 mM $CaCl_2$. Resonances shifted at different conditions are labeled by arrows.

perturbed by the addition of Ca^{2+}, but several residues, such as D15, D17, I18, N60, D62, and L63, experience significant changes in their chemical shifts (Figure 2). No such changes are observed upon the addition of 130 mM KCl. Moreover, the host protein does not exhibit any significant Ca^{2+}-induced chemical shift changes. Figure 2b displays the concurrent change of the NH chemical shifts of these residues as a function of Ca^{2+} with a K_d for Ca^{2+} of 1.4 ± 0.4 mM. The changes in chemical shifts of residues at the designed Ca^{2+}-binding pocket clearly indicate that Ca^{2+} binds to the designed Ca^{2+}-binding site.

Tb^{3+} has binding properties similar to those of Ca^{2+} and has been widely used as a probe for Ca^{2+}-binding proteins.[24] The proximity (7.2 Å) of the metal ion to W32 (Figure 1a) enables us to detect Tb^{3+} binding by fluorescence resonance energy transfer between the aromatic residue and the bound terbium. As shown in Figure 3a, the addition of Ca·CD2 into a fixed concentration of terbium results in the enhancement of the terbium fluorescent signal at 545 nm, indicating the formation of a Tb^{3+}−Ca·CD2 complex. Further, Tb^{3+} fluorescence enhancement with the addition of Tb^{3+} in a fixed Ca·CD2 concentration reached saturation at about 70 μM Tb^{3+}. The addition of Tb^{3+} to CD2 does not lead to a significant change of Tb^{3+} fluorescence enhancement (the same aromatic residues

(24) Horrocks, W. D., Jr. *Adv. Inorg. Biochem.* **1982**, *4*, 201−261.

responsible for FRET observed in Ca·CD2 are present in CD2). By monitoring the change of Tb^{3+} fluorescence enhancement as a function of Tb^{3+} concentration, we obtained the Tb^{3+}-binding affinity of Ca·CD2 ($K_d = 6.6 \pm 1.6$ μM) (Figure 3b). Using the Tb^{3+} fluorescence, a competition assay was completed by increasing the La^{3+} concentration with constant Tb^{3+} and Ca·CD2 concentrations. The metal-binding affinity for La^{3+} is 5.0 ± 1.6 μM (K_d). The metal affinities of Ca·CD2 for La^{3+} and Tb^{3+} are very similar and are more than 200 times higher than that of Ca^{2+} under similar conditions. Lack of the metal-dependent conformational change and the high solvent accessibility of the metal-binding site suggest that this large affinity difference between the Ca^{2+} and Ln^{3+} ions mainly results from the different properties of the metal ions, such as the charge numbers and ionic radii. In-depth analysis of this affinity difference, including the influences from the protein environment and local coordination shell, will be pursued using our design approach in the future.

Like natural Ca^{2+}-binding proteins, Ca·CD2 also exhibits a good selectivity for Ca^{2+} under physiological conditions of Mg^{2+} (3−10 mM) and K^+ (130 mM). The 1D ^{1}H NMR spectra of Ca·CD2 with sequential addition of EGTA (0.050 mM), K^+ (130 mM), Mg^{2+} (10 mM), and Ca^{2+} (5 mM) are shown in Figure 3d,e. Ca^{2+}-induced changes clearly do not result from the presence of high salt. These changes can be assigned to the residues close to the Ca^{2+}-binding site in the protein. Ca^{2+} and La^{3+} are also able to compete with Tb^{3+} for binding to the designed Ca^{2+}-binding site (Figure 3c). The specific binding for K^+ and Mg^{2+} of the designed metal-binding site is too weak to be detected under our experimental conditions. These results clearly demonstrate that Ca·CD2 is able to bind Ca^{2+} with good selectivity over excess mono- and divalent ions.

Structural Determination. To evaluate the high-resolution features of the design, the solution structure of Ca·CD2 has been determined by homonuclear and heteronuclear multidimensional NMR spectroscopy. Structural calculations were performed with the CNS program using standard annealing protocols.[25] The solution structure of Ca·CD2 was first modeled without any constraints on the Ca^{2+} and ligand oxygen atoms (see Supporting Table 1). On the basis of the statistical results from the crystal structures, the average Ca−O distance in the Ca^{2+}-binding proteins is approximately 2.4 Å with an upper limit of more than 3 Å. Therefore, a group of oxygen atoms that coordinates one Ca^{2+} ion should be in a distance range of less than 6 Å. Supporting Table 2 shows the O−O distances of the designed ligands in the 20 lowest-energy models of 100 structures without constraints on Ca^{2+}. It is noted that the O−O distances of the side chains from D15, D17, N60, and D62 frequently fall into the range for formation of a Ca^{2+}-binding pocket. Sixteen of the twenty models have more than four oxygen atoms from the designed ligands positioned together for possible Ca^{2+} binding. In addition, the aspartate residues have been used as the bidentate ligands in the models, suggesting there is room for holding more oxygen atoms around the possible Ca^{2+} position. The O−O distances of the neighboring main chain carbonyls and the side chain of other residues (such as I18, F21, Q22, and L63) with significant changes of their chemical shifts (Figure 4a,b) were also measured, but they are out of the required range for a Ca^{2+}-binding pocket (>8 Å, data not shown).

Therefore, in the final structural calculation, five additional constraints, with the Ca−O distance set from 1.8 to 2.8 Å for the OD1 of all four ligand residues and one OD2 of either D15, D17, or D62, were included. The backbone is well defined with an almost identical root-mean-square (rms) deviation for the 20 lowest structures with and without the Ca^{2+} constraints (Table 1 and Supporting Table 1), as revealed by MolMol. The restraints improved the convergence in the conformations of the side chains involving a Ca^{2+} ligand and appear to have no significant effect on the structures obtained without Ca^{2+}. When the designed ligand residues are constrained to Ca^{2+} with either unidentate or bidentate carboxyl oxygen atoms, 9 and 12 out of the 20 lowest-energy structures are found to use the bidentate residues from D15 and D62, respectively. In contrast, D17 was not used as a bidentate ligand residue. This final calculated Ca^{2+}-binding mode agrees with the results from Mn^{2+}-induced relaxation effects on the ^{1}H−^{15}N HSQC cross-peaks.

Table 1 summarizes the structural parameters of the final solution structure of Ca·CD2. The structure was determined from 1136 experimental constraints and 5 Ca^{2+} constraints. The experiment constraints include 1064 NOE distance constraints and 36 hydrogen bonds. The backbone is well defined with a root-mean-square (rms) deviation from the mean of 0.33 Å. The stereochemical quality of the ensemble of structures was examined using PROCHECK,[26] and it indicated that 98.4% of the residues are in the most favored and allowed regions of the Φ−Ψ space. With the exception of the disordered N-terminal

Table 1. NMR Structural Statistics for the Final Lowest-Energy Structures of Ca·CD2 (residues 5−99) in the Presence of 10 mM $CaCl_2$

Constraints	
total NOEs	1064
intraresidue	415
sequential	262
short range ($\|i-j\| \leq 4$)	92
long range ($\|i-j\| > 4$)	295
Ca	5
H-bonds	36
Procheck Statistics	
most favored regions	77.58%
allowed regions	20.86%
generously allowed regions	0.96%
disallowed regions	0.60%[a]
CNS Statistics[b]	
total energy (kcal/mol)[c]	193 ± 2
NOE energy (kcal/mol)[c]	65 ± 2
bond lengths (Å)	0.00246 ± 0.00002
bond angles (deg)	0.409 ± 0.002
improper (deg)	0.264 ± 0.002
RMS Deviation from the Average Structures (Å)	
backbone	0.331
all heavy atom	0.897
Ca−O Distance (Å)[b]	
D15 (the one closer to calcium)	2.686 ± 0.045
D17	2.808 ± 0.001
N60	2.807 ± 0.001
D62 (the one closer to calcium)	2.351 ± 0.051
second O from D15 or D62	2.881 ± 0.027

[a] Lys-45 at the loop region with few restraints. [b] Value shown as rms ± rmsd. [c] Two NOE constraints for Lys-45 have a looser limitation (compare to the structures without Ca^{2+}; see Supporting Table 1).

(25) Brunger, A. T.; Adams, P. D.; Clore, G. M.; DeLano, W. L.; Gros, P.; Grosse-Kunstleve, R. W.; Jiang, J. S.; Kuszewski, J.; Nilges, M.; Pannu, N. S.; Read, R. J.; Rice, L. M.; Simonson, T.; Warren, G. L. *Acta Crystallogr. D* **1998**, *54*, 905−921.

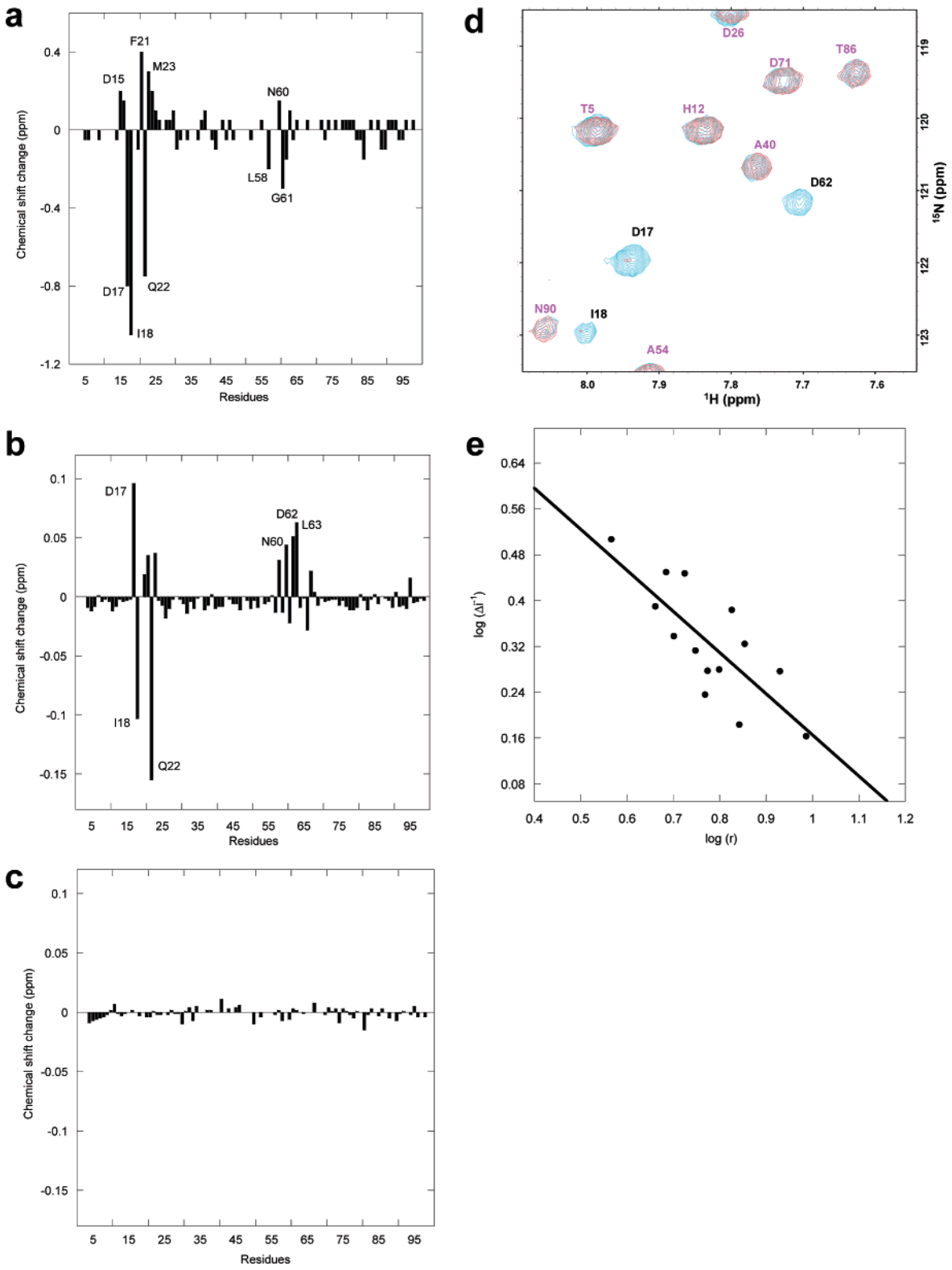

Figure 4. Ca^{2+}-binding mode of Ca·CD2. (a) Differences in ^{15}N chemical shifts for the backbone nitrogen atoms between the Ca^{2+}-loaded and the Ca^{2+}-free forms derived from the $^{1}H-^{15}N$ HSQC spectra of Ca·CD2. The NMR assignments of the Ca·CD2 with and without Ca^{2+} have been deposited in BioMagResBank (http://www.bmrb.wisco.edu) under accession number 6201. (b) Differences in the ^{1}H chemical shifts of the backbone amide protons of Ca·CD2 derived from the $^{1}H-^{15}N$ HSQC and $^{1}H-^{1}H$ TOCSY spectra between the Ca^{2+}-loaded (10 mM $CaCl_2$) and the Ca^{2+}-free (3 mM EGTA) forms. (c) Differences in the ^{1}H chemical shifts of the backbone amide protons for CD2 derived from the $^{1}H-^{1}H$ TOCSY spectra collected under the same conditions as Ca·CD2. (d) $^{1}H-^{15}N$ HSQC spectra of Ca·CD2 in 50 mM PIPES/130 mM KCl/1 mM $CaCl_2$, pH 6.8, with (red) and without (cyan) Mn^{2+} (50 μM) at 4 °C. (e) Correlation between Mn^{2+}-induced effects on $^{1}H-^{15}N$ HSQC cross-peak intensities of residues 14−18 and 58−65 and distances between the amide protons of these residues and the Ca^{2+} ion in the designed Ca^{2+}-ion-binding site. Logarithmic plot of the changes in the inverted intensities of $^{1}H-^{15}N$ HSQC cross-peaks induced by 20 μM Mn^{2+} versus amide proton/metal-binding site distances[28] in 50 mM PIPES in the absence of Ca^{2+}, validating the designed Ca^{2+}-binding mode. The metal−NH distances were obtained from the average structure of Ca·CD2 (deposited in protein data bank, code 1T6W).

four residues, the structure of Ca·CD2 is well ordered with respect to the expected IG-fold. Comprehensive evaluation of more than 30 structural parameters, both for individual residues and the entire protein, using the VADAR web server,[27] has confirmed the quality of the calculated structure. Ca·CD2 has a structure very similar to that of CD2 observed by CD, fluorescence, and NMR studies (see Supporting Figures 1 and 2). The average minimized structure of Ca·CD2 and the structure of CD2 (1hng) have a root-mean-square (rms) deviation of 1.047 Å for the backbone (see Supporting Figures 3 and 4). The aromatic residues in the hydrophobic core are tightly packed with no substantial alterations resulting from the introduction of the Ca^{2+}-binding site.

Calcium-Binding Mode. The structural calculations have been performed both with and without constraints to Ca^{2+}. As shown in Table 1, the Ca^{2+} constraints set at a Ca−O distance of 2.8 Å (1.8−2.8 Å) are well accommodated in the structural calculations (violations less than 0.1 Å). The constraints improved the convergence in the conformations of the side chains of residues that serve as Ca^{2+} ligands and appear to cause no significant deviations from the structures obtained without Ca^{2+} (see Supporting Table 1). Among the 20 lowest-energy structures calculated without Ca^{2+} restraints, the O−O distances between the designed Ca^{2+} ligand residues of D15, D17, N60, and D62 were often observed to be less than 6 Å (see Supporting Table 2). These results are consistent with the designed pentagonal bipyramidal geometry that considers bond length and angle deviations. When constraints to Ca^{2+} are included, D15 or D62 serves as a bidentate ligand in all of the 20 lowest-energy structures.

To examine whether the Ca^{2+}-binding mode of Ca·CD2 (Figure 1) agrees with our design, three different approaches, including NMR chemical shift differences of individual nuclei between Ca^{2+}-free and Ca^{2+}-loaded forms, site-directed mutagenesis, and Mn^{2+}-induced relaxation experiments, were conducted. As shown in Figure 4a−c, Ca^{2+} induces changes greater than 0.75 ppm in the ^{15}N chemical shift of the D17, I18, and Q22 backbone nitrogens. Nine residues (15−16, 21, 23−24, 58, 60−62) also experience significant backbone ^{15}N chemical shift changes (0.2−0.4 ppm). The remaining residues exhibit Ca^{2+}-induced ^{15}N chemical shift changes of less than 0.1 ppm. For the backbone amide protons, the Ca^{2+}-induced ^{1}H chemical shift changes of D17, I18, and Q22 are up to 0.1 ppm, while most of the Ca^{2+}-induced changes are less than 0.02 ppm. The other residues exhibiting significant Ca^{2+}-induced amide proton chemical shift changes are N20, F21, M23, L58, N60, D62, and L63. All of these residues with significant chemical shift changes in the backbone ^{15}N and amide protons are either the proposed ligands for Ca^{2+} binding or the nearby residues. The analyses of other protons, such as CαH, result in the same conclusion. In contrast, no significant chemical shift changes in wild-type CD2 are observed upon addition of Ca^{2+}.

Second, site-directed mutagenesis was applied to further clarify whether D15 and Q22 are involved in the Ca^{2+} binding. It was noticed that D15 has relatively small changes in the chemical shifts between the Ca^{2+}-free and -loaded forms although it was designed to directly chelate Ca^{2+} in the designed site, while Q22, which is not a designed ligand, has the greatest chemical shift change (Figure 4). Consistent with our design, the mutant D15A completely removed Tb^{3+}-binding affinity, while the mutant Q22A retains the full metal-binding ability of Ca·CD2, confirming that Q22 in Ca·CD2 is not directly involved in the Ca^{2+} binding. These data strongly suggest that Ca^{2+} specifically binds to Ca·CD2 at the designed Ca^{2+}-binding site. The relatively large change in chemical shifts of Q22 at the flexible loop is likely due to the local conformational change upon Ca^{2+} binding.

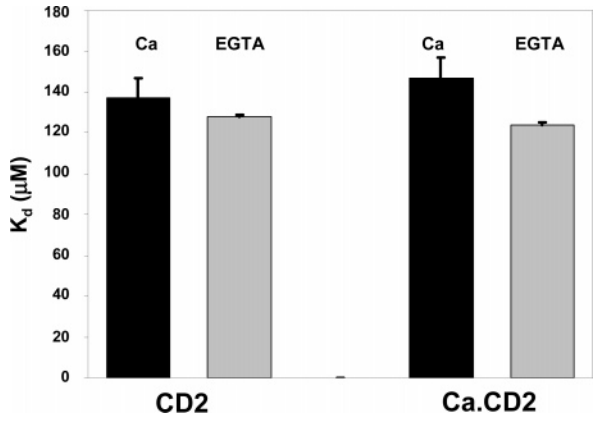

Figure 5. Dissociation constants for CD2 (left) and Ca·CD2 (right) binding to CD48 in the presence of 10 mM $CaCl_2$ (black bar) or 1 mM EGTA (gray bar) from surface plasmon resonance measurements using a Biacore instrument. Errors are shown as standard errors of the mean.

Third, to determine more accurately the location of the Ca^{2+}-binding site, we monitored Mn^{2+}-induced relaxation of amide protons using $^{1}H-^{15}N$ HSQC spectroscopy. Paramagnetic Ca^{2+} analogues, such as Mn^{2+}, are expected to have strong relaxation effects on nuclei in their proximity.[28] Figure 4d shows that the amide groups of I18, D17, and D62 in the Ca^{2+}-binding pocket significantly decrease in cross-peak intensities (Δi) upon addition of Mn^{2+}. The log Δi^{-1} exhibits the expected linear relationship with respect to $HN-Ca^{2+}$ distance calculated from the Ca^{2+}-loaded structures, validating the Ca^{2+}-binding mode (Figure 4e and Supporting Figure 5).

Cell Adhesion Function. To investigate the effect of designed Ca^{2+}-binding sites on the biological function of CD2, we measured the Ca·CD2-binding affinity to sCD48 by surface plasmon resonance in the absence and presence of Ca^{2+}. As shown in Figure 5, the dissociation constant of Ca·CD2 for CD48 is very similar to that of CD2. Antibodies OX34 and OX55 recognize specific regions of CD2 (D28 and E29 and E41 and R70, respectively). Using CD2 as the control (100%), the binding of Ca·CD2 to the conformation-dependent antibody OX34 is 104 and 106% with Ca^{2+} and EGTA, respectively. The binding to OX55 is 90 and 101% with Ca^{2+} and EGTA, respectively. These results strongly suggest that Ca·CD2 retains its native biological ability to bind to CD48. It is interesting to note that Ca^{2+} binding to Ca·CD2 decreases the binding affinity to CD48 by approximately 15%, although this designed site is located on the surface opposite from the CD48 recognition site. The binding of soluble CD48 results in significant changes in chemical shifts and line broadening of a few residues at the C and C′ strands of domain 1 of CD2, as reported by Driscoll

(26) Laskowski, R. A.; Rullmannn, J. A.; MacArthur, M. W.; Kaptein, R.; Thornton, J. M. *J. Biomol. NMR* **1996**, *8*, 477−486.
(27) Willard, L.; Ranjan, A.; Zhang, H.; Monzavi, H.; Boyko, R. F.; Sykes, B. D.; Wishart, D. S. *Nucleic Acids Res.* **2003**, *31*, 3316−3319.
(28) Mildvan, A. S.; Cohn, M. *Adv. Enzymol. Relat. Areas Mol. Biol.* **1970**, *33*, 1−70.

and colleagues.[29] Although L63 is not located at the functional surface, upon binding to CD48, nuclei in this residue exhibit substantial chemical shift changes that are comparable to those of functional surface residues. The decrease in affinity of CD48 for Ca·CD2 in the presence of Ca^{2+} may be a result of the local conformational change of Ca·CD2 caused by the perturbation of long-range electrostatic interactions.

Conclusions

In summary, we have demonstrated a successful strategy for designing Ca^{2+}-selective binding sites in proteins with desired structural and cell adhesion function. The structural information provides a close view of structural determinants that are necessary for a functional protein to accommodate the metal-binding site. Ca·CD2 is an excellent model system for studying the contribution of key determinants to Ca^{2+}-binding affinity and selectivity, as well as the mechanism of cell adhesion.[15] In addition, it represents a major achievement toward understanding Ca^{2+} signaling and designing functional proteins that can be controlled by Ca^{2+} binding. Since the designed metal-binding proteins exhibit a high affinity to lanthanide and other paramagnetic metal ions, they have strong applications in facilitating structure determination of large protein complexes from the known structures of the component proteins using docking protocols based on residual dipolar couplings.[30] Furthermore, the developed design strategy can be used for creating other novel metal-selective and metal-sensitive functional proteins or enzymes and for the construction of new biomaterials, sensors, catalysts, and pharmaceuticals.[22,31−34]

Acknowledgment. We thank Charles Louis, Michael Gross, Giovanni Gadda, Dan Adams, and Bonnie Fritz for the critical review of this manuscript and helpful discussions. We thank Michael Kirberger for the program PROTEUS, Sarah Shealy for MS, John Glushka for NMR, and other members in Jenny J. Yang's research group for their helpful discussions. This work is supported in part by the NIH and NSF grants to J.J.Y., and NIH predoctoral fellowship to A.L.W.

Supporting Information Available: Circular dichroism, fluorescence, NMR, and structure comparison results, and two tables summarizing the structure calculation. This material is available free of charge via the Internet at http://pubs.acs.org.

JA0431307

(29) McAlister, M. S.; Mott, H. R.; van der Merwe, P. A.; Campbell, I. D.; Davis, S. J.; Driscoll, P. C. *Biochemistry* **1996**, *35*, 5982−5991.
(30) Barbieri, R.; Bertini, I.; Cavallaro, G.; Lee, Y. M.; Luchinat, C.; Rosato, A. *J. Am. Chem. Soc.* **2002**, *124*, 5581−5587.
(31) DeGrado, W. F.; Summa, C. M.; Pavone, V.; Nastri, F.; Lombardi, A. *Annu. Rev. Biochem*. **1999**, *68*, 779−819.
(32) Looger, L. L.; Dwyer, M. A.; Smith, J. J.; Hellinga, H. W. *Nature* **2003**, *423*, 185−190.
(33) Kuhlman, B.; Dantas, G.; Ireton, G. C.; Varani, G.; Stoddard, B. L.; Baker, D. *Science* **2003**, *302*, 1364−1368.
(34) Oliynyk, Z.; Briseno-Roa, L.; Janowitz, T.; Sondergeld, P.; Fersht, A. R. *Protein Eng. Des. Sel.* **2004**, *17*, 383−390.
(35) Koradi, R.; Billeter, M.; Wuthrich, K. *J. Mol. Graph.* **1996**, *14*, 51−55.
(36) Kraulis, P. J. *J. Appl. Cryst.* **1991**, *24*, 946−950.